CHEMISTRY
A EUROPEAN JOURNAL

DOI: 10.1002/chem.201001236

Hydroxyl Radical Reactions with Adenine: Reactant Complexes, Transition States, and Product Complexes

Qianyi Cheng,[a] Jiande Gu,[b] Katherine R. Compaan,[a] and Henry F. Schaefer, III*[a]

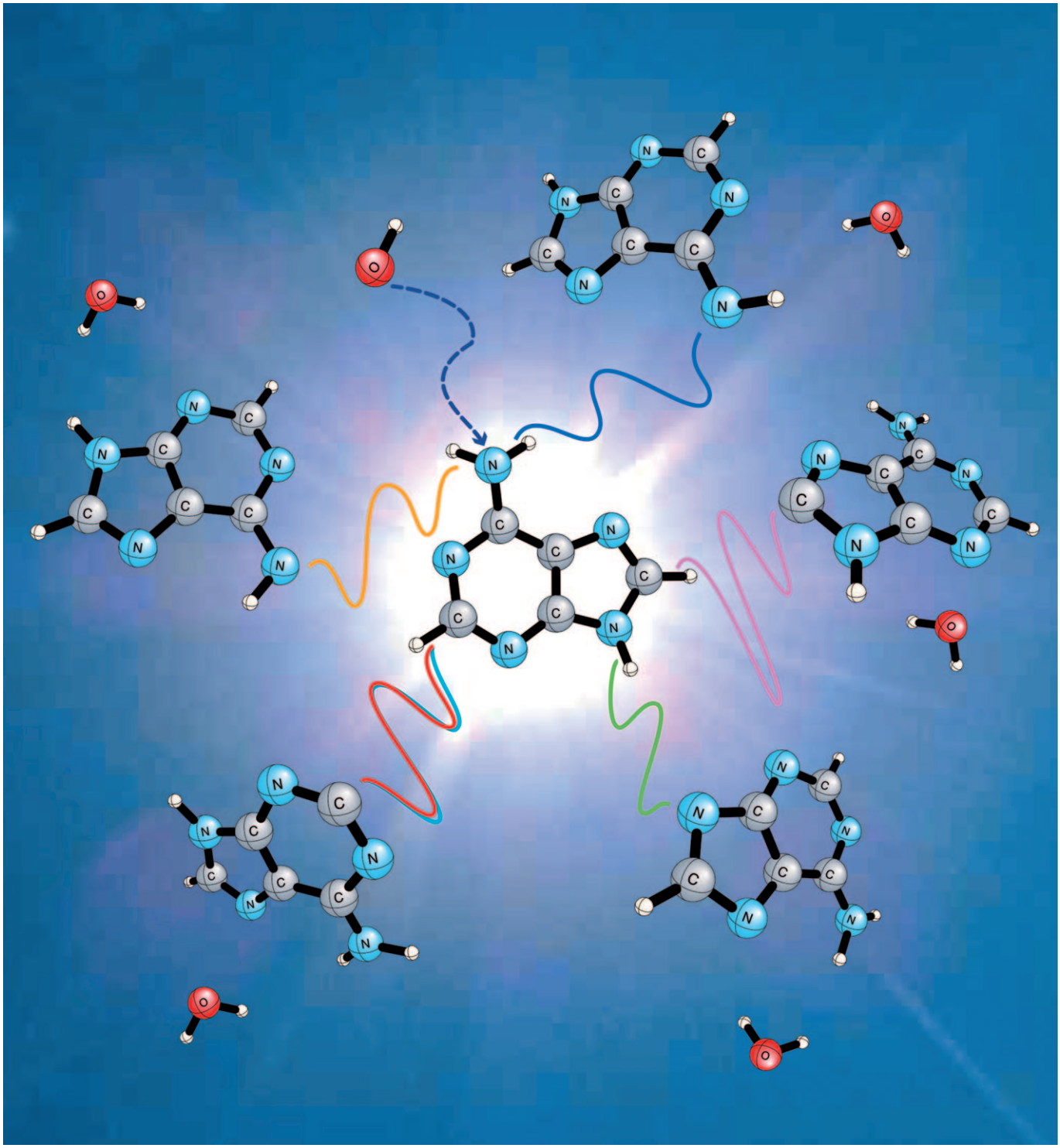

Abstract: In order to address problems such as aging, cell death, and cancer, it is important to understand the mechanisms behind reactions causing DNA damage. One specific reaction implicated in DNA oxidative damage is hydroxyl free-radical attack on adenine (A) and other nucleic acid bases. The adenine reaction has been studied experimentally, but there are few theoretical results. In the present study, adenine dehydrogenation at various sites, and the potential-energy surfaces for these reactions, are investigated theoretically. Four reactant complexes [A···OH]• have been found, with binding energies relative to A+OH• of 32.8, 11.4, 10.7, and 10.1 kcal mol^{-1}. These four reactant complexes lead to six transition states, which in turn lie +4.3, −5.4, (−3.7 and +0.8), and (−2.3 and +0.8) kcal mol^{-1} below A+OH•, respectively. Thus the lowest lying [A···OH]• complex faces the highest local barrier to formation of the product (A−H)•+H_2O. Between the transition states and the products lie six product complexes. Adopting the same order as the reactant complexes, the product complexes [(A−H)···H_2O]• lie at −10.9, −22.4, (−24.2 and −18.7), and (−20.5 and −17.5) kcal mol^{-1}, respectively, again relative to separated A+OH•. All six A+OH• → (A−H)•+H_2O pathways are exothermic, by −0.3, −14.7, (−17.4 and −7.8), and (−13.7 and −7.8) kcal mol^{-1}, respectively. The transition state for dehydrogenation at N_6 lies at the lowest energy (−5.4 kcal mol^{-1} relative to A+OH•), and thus reaction is likely to occur at this site. This theoretical prediction dovetails with the observed high reactivity of OH radicals with the NH_2 group of aromatic amines. However, the high barrier (37.1 kcal mol^{-1}) for reaction at the C_8 site makes C_8 dehydrogenation unlikely. This last result is consistent with experimental observation of the imidazole ring opening upon OH radical addition to C_8. In addition, TD-DFT computed electronic transitions of the N_6 product around 420 nm confirm that this is the most likely site for hydrogen abstraction by hydroxyl radical.

Keywords: adenine · dehydrogenation · density functional calculations · radical reactions

Introduction

Cellular DNA contains the complex hereditary information of living organisms. Organisms must maintain the integrity of their DNA in order to remain healthy and propagate. Both normal metabolic activities, and environmental effects can damage DNA.[1–28] When damage accumulates to the extent that it can no longer be repaired, three major problems may occur. These are senescence, programmed cell death, and carcinogenesis, and are manifested by aging, neurological syndromes, and cancer. Thus, the identification and repair of DNA damage is an important factor in improving human health and longevity. A tremendous amount of research has focused on the causes of DNA damage, both exogenously and endogenously. Oxidative damage of cellular DNA by free radicals may be a significant factor in human carcinogenesis.[29–33] There are several reactive oxygen species commonly present in biological systems. Of these, hydroxyl free radical (•OH) appears to be the most damaging.[30,34,35] Normally, hydroxyl radical is present at low concentrations, due to the metabolism of oxygen. Higher concentrations are caused by respiratory bursts, or acute exposure to oxidizing agents such as ionizing radiation[36] or UVA solar light.[37] Solar radiation is strongly implicated in the induction of human skin cancers, including squamous cell and basocellular carcinoma, along with malignant melanoma.[37]

Approximately half of the damage caused by OH radicals occurs on nucleobases. Nucleobases are the structural units which carry genetic information in DNA and RNA. The five principal nucleobases are guanine (G), cytosine (C), adenine (A), thymine (T), and uracil (U). Thymine is only present in DNA, while only RNA contains uracil. Of the four DNA nucleobases, guanine is the most likely to be attacked by OH radicals. The probability that guanine will suffer an initial •OH attack is 36%, while adenine, thymine, and cytosine have initial attack probabilities of 24, 22, and 18%, respectively.[38] Because of this, the one-electron oxidation of guanine is of great interest, particularly oxidation by OH radical. The gas-phase dehydrogenation reaction of guanine with OH radical was studied by Colvin and co-workers[19] using Car–Parinello molecular dynamics in 2002. N_{11} is predicted to be the most favorable site for dehydrogenation. Guanine can under go •OH addition at its C_4 or C_8 positions; however, this is less favorable than N_{11} dehydrogenation. Of the two addition products, the C_8-hydroxylated radical is more stable. Compared to the N_{11} dehydrogenation product, the N_9 dehydrogenated product lies 1.9 kcal mol^{-1} higher in energy, and the N_1 dehydrogenated product is 3.4 kcal mol^{-1} higher. Dehydrogenation at C_8 is strongly disfavored, being 26.9 kcal mol^{-1} higher in energy at the B3LYP/6-31++G-(3df,3pd) level. The free-energy dehydrogenation reaction barrier is predicted to be lowest for N_9 (0.15 kcal mol^{-1}), fol-

[a] Q. Cheng, K. R. Compaan, Prof. H. F. Schaefer, III
Center for Computational Quantum Chemistry
University of Georgia, Athens, GA 30602 (USA)
Fax: (+1) 706-542-0406
E-mail: fri@uga.edu

[b] J. Gu
Discovery Center, State Key Laboratory of Drug Research
Shanghai Institute of Materia Medica
Shanghai Institutes for Biological Sciences
CAS, Shanghai 201203 (P. R. China)

lowed by N_{11} (0.86 kcal mol^{-1}) and C_8 (9.64 kcal mol^{-1}). Because of the low barriers for N_9 and N_{11}, these reactions may occur spontaneously, even at low temperatures. For the C_8 position, dehydrogenation occurs at a reasonable rate at room temperature but would be slow at low temperatures.

In more recent work, Chatgilialoglu and co-workers experimentally studied the reaction of the OH radical with guanosine and 8-bromoguanosine using absorption spectroscopy, in an effort to reevaluate the ambient reactivity of guanine moieties toward ·OH radicals.[39] A broad band at 616 nm implies that the major reaction between guanine and the OH radical is hydrogen abstraction from NH_2, followed by tautomerization. Hydroxyl radical addition at the C_4 position is less important.

There is controversy concerning Chatgilialoglu's interpretation of his guanine experiments.[39] Previous studies indicated ·OH radical adds to the C_4, C_5, or C_8 positions on purine bases and their derivatives.[40,41] These hydroxylated radicals and the subsequent ring-opening or dehydration reactions have been characterized by their redox properties.[17,42,43] Even though direct hydrogen abstraction by ·OH radical may not, at present, be known to be the predominant reaction with guanine, it is important to study all the ways in which free radicals can cause oxidative DNA damage.

Adenine has the second highest initial ·OH attack probability, so it is also of great interest. Hydroxyl radical typically adds to the double bonds of adenine to yield C_4, C_5, and C_8 radical adducts.[40,41,44–46] Of these three products, the A4OH radical constitutes more than 81% of the hydroxylated radicals generated.[41] The A4OH radical adduct is a weak oxidant. However, like guanine, A4OH can lose a water molecule and become a strong oxidant, the (A−H)· radical. The second most abundant radical product is A8OH, which comprises about 18% of the radicals generated.[41] This radical is actually predicted to form the products 8-hydroxyadenine, 5-formamido-4,6-diaminopyrimidine (FAP_Y), (FAP_YG), and 5′-cyclo-2′-deoxy-adenosine.[40] Vieira and Steenken studied the transient species formed during the aqueous reaction of OH radical with adenine. Using a combination of conductance, optical detection, and absorption spectroscopy, they monitored the reaction of the OH radical with fully alkylated adenines, such as N^6, N^6-dimethyladenosine, and N^6, N^6, 9-trimethyladenine.[44] Either dehydroxylation or dehydration can occur when OH radicals add at C_4 or C_5 sites. This is evidenced by a decrease in optical density (OD) at 400 nm. If the OH radicals add at the C_8 site, ring-opening occurs and the OD at 330 nm increases. A 2008 study by Naumov and Sonntag[46] confirmed the earlier indications that OH radicals form an adduct with adenine at the C_4 position. The adduct undergoes proton or hydrogen transfer, followed by dehydration, to form an N_6-dehydrogenated radical. On the other hand, if the C8 adduct is formed, ring-opening occurs. The product is 5-formamido-4,6-diaminopyrimidine (FAP_Y). X-ray radiation[4,47–50] or OH radicals[40,41] can attack the C_2, C_8, N_9, N_{61}, or N_{62} positions directly, producing neutral radicals or ionized species.[46,51]

In the realm of quantum chemistry, a plethora of highly interesting large systems have not yet been explored, including many DNA subunits. For sufficiently small species, wave function methods yield excellent results, accurate to within 1 kcal mol^{-1}.[52,53] This chemical accuracy is only possible for systems with a limited number of chemically active electrons. On the other hand, density functional theory (DFT) holds promise for very large systems.[54,55] It is typically more accurate than Hartree–Fock theory and semi-empirical methods, but is efficient enough to be applied to large molecules. Because of this, DFT is an effective method for quantum chemistry applications.

Neutral adenine[56] and five dehydrogenated adenine radical derivatives[57] have been considered in previous theoretical studies. However, the mechanisms of crucial dehydrogenation reactions have not been fully unravelled. Specifically, the energetics and associated transition states for dehydrogenation of adenine by OH radical (A + ·OH → ·A−H + H_2O) are not known. The present study elucidates the potential energy surfaces for dehydrogenation of adenine by ·OH radical. The corresponding reaction pathways and energetics are provided, and should shed light on related biochemical experiments.

Computational Methods

The generalized gradient approximation exchange-correlation B3LYP functional was employed in this work. This method has predicted reasonable results for DNA bases, base pairs, and anions[58–61] in previous research. This functional is a combination of Becke's 3-parameter HF/DFT hybrid exchange functional (B3)[62] with the dynamical correlation functional of Lee, Yang, and Parr (LYP).[63]

The B3LYP method is adopted along with double-ζ quality basis sets with polarization and diffuse functions (denoted as DZP++). The DZP++ basis sets are created by augmenting the Huzinaga-Dunning set of contracted double-ζ Gaussian functions with one set of p-type polarization functions for each H atom and one set of five d-type polarization functions for each first-row atom. To complete the DZP++ basis, one even-tempered s diffuse function was added to each H atom, while even-tempered s and p diffuse functions were centered on every heavy atom. The even-tempered orbital exponents were determined according to the prescription of Lee [Eq. (1)],[64] in which α_1, α_2, and α_3 are the three smallest Gaussian orbital exponents of the s- or p-type primitive functions for a given atom ($\alpha_1 < \alpha_2 < \alpha_3$).

$$\alpha_{diffuse} = \frac{1}{2}\left(\frac{\alpha_1}{\alpha_2} + \frac{\alpha_1}{\alpha_2}\right)\alpha_1 \quad (1)$$

The final DZP++ set contains six functions per H atom (5s1p/3s1p) and nineteen functions per C, N, or O atom (10s6p1d/5s3p1d). There are 220 contracted functions for the adenine molecule, 245 functions for adenine-OH complexes, and 214 functions for dehydrogenated adenine molecules. This combination of functionals and basis sets has the tactical advantage that it has previously been used in comprehensive benchmark studies[65] of a wide range of electron affinities.

The binding energies for reactant complexes (A···OH)· (BE1) and for product complexes [(A−H)···H_2O]· (BE2) were evaluated according to the following definitions given in Equations (2) and (3).

$$BE1 = E(A) + E(OH^{\bullet}) - E[(A \cdots OH)^{\bullet}] \quad (2)$$

$$BE2 = E(A) + E(OH^{\bullet}) - E[^{\bullet}(A{-}H) \cdots H_2O] \quad (3)$$

The dissociation energy for reactant complexes (A···OH)• (DE1) and for product complexes [(A–H)···H_2O]• (DE2) were evaluated according to the following definitions given in Equations (4) and (5).

$$DE1 = E[(A-H)^{\bullet}] + E(H_2O) - E[(A\cdots OH)^{\bullet}] \quad (4)$$

$$DE2 = E[(A-H)^{\bullet}] + E(H_2O) - E[^{\bullet}(A-H)\cdots H_2O] \quad (5)$$

Computations of optimized geometries, harmonic vibrational frequencies, natural populations,[66–68] and intrinsic reaction coordinates (IRC)[69–72] were performed with the QChem package,[73] which was also used for time-dependent DFT (TD-DFT) treatment of excited electronic states.

Results and Discussion

The structure and numbering scheme for adenine are shown in Figure 1. The optimized geometries of neutral adenine molecule, hydroxyl radical, and neutral water molecule are

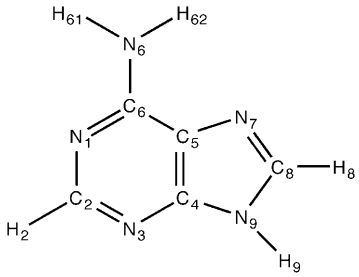

Figure 1. IUPAC numbering of atoms for adenine.

displayed in Figure 2. The optimized geometries of dehydrogenated adenine radicals in the isolated forms are shown in Figure 3. The stability sequence of these radicals is A–H_9 > A–H_{62} > A–H_{61} > A–H_2 > A–H_8. Microhydration with one water molecule in the dehydrogenation reactions does not change this stability order. The relative energies are summarized in Table 1. The N_9-dehydrogenated adenine is the

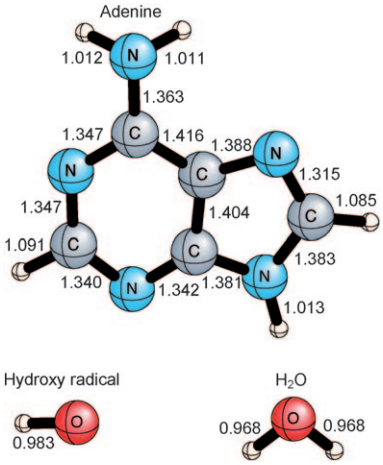

Figure 2. Optimized geometries of isolated adenine, hydroxyl radical and water, with bond lengths in Å.

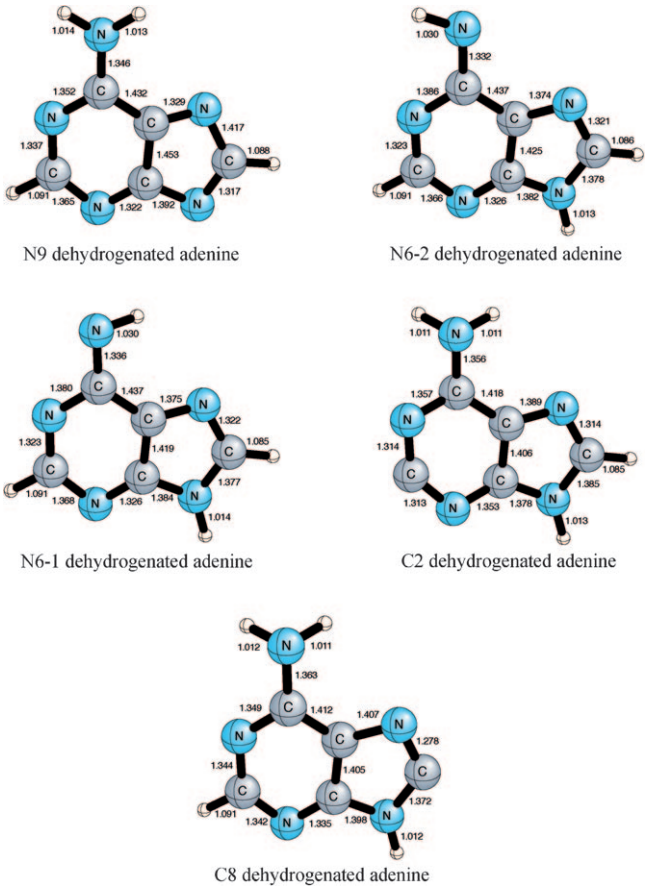

Figure 3. Five optimized structures for (A–H) radicals, that is, structures resulting from the removal of one hydrogen atom from adenine. Bond lengths are in Å.

Table 1. Energies (ΔE, in kcal mol^{-1}, ZPVE corrected values in parentheses) of the five dehydrogenated adenine radicals [(A–H)•] plus water, relative to separated adenine plus OH radical. Also reported are reaction enthalpies (ΔH, in kcal mol^{-1}), entropies (ΔS, in cal mol^{-1}), and Gibbs energies (ΔG, in kcal mol^{-1}) for A + OH• → (A–H)• + H_2O.

	ΔE	ΔH	ΔS	ΔG
N_9-dehydrogenated adenine	−17.36 (−17.88)	−0.30	3.33	−1.30
N_{62}-dehydrogenated adenine	−14.75 (−15.27)	−0.53	2.07	−1.14
N_{61}-dehydrogenated adenine	−13.67 (−14.20)	−0.54	2.04	−1.15
C_2-dehydrogenated adenine	−7.85 (−8.06)	0.24	5.28	−1.34
C_8-dehydrogenated adenine	−0.30 (−0.43)	0.24	4.04	−0.96

most stable radical, followed by the two N_6-dehydrogenated products. Dehydrogenation reactions at nitrogen sites are all exothermic, with enthalpy changes of −0.30 for N_9, −0.54 for N_{61}, and −0.53 kcal mol^{-1} for N_{62}. Carbon site dehydrogenated adenine radicals are much higher in energy (9.52 (9.82) for C_2 site, 17.06 (17.46) kcal mol^{-1} for C_8 site) than the N_9-radical. In addition, at the carbon site, these dehydrogenation reactions are endothermic; the enthalpy changes are both 0.24 kcal mol^{-1}. Nevertheless, the changes in the Gibbs energy for all six dehydrogenation reactions are negative (−1.34, −0.96, −1.30, −1.15 and −1.14 kcal mol^{-1} for

C_2, C_8, N_9, and two N_6 sites, respectively) at room temperature. Thus, these reactions are thermodynamically favored.

A natural population analysis (NPA) for neutral adenine is presented in Figure 4. Adenine has five hydrogen atoms.

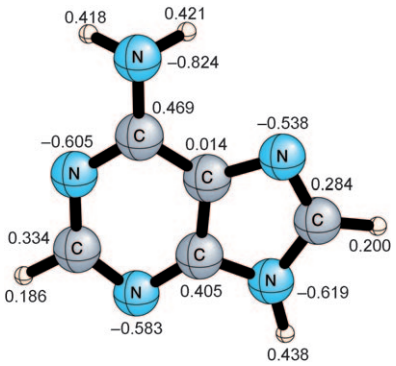

Figure 4. Natural population analysis (NPA) for neutral adenine.

Three of these H atoms are attached to C_2, C_8, and N_9, while two bond to N_6. From Figure 4, it is clear that hydrogens bound to nitrogen atoms (N_6 and N_9) are more positively charged. The positive charges on the five hydrogen atoms are in this order: $H_9 > H_{62} > H_{61} > H_8 > H_2$. Thus, all hydrogen atoms are vulnerable to OH radical attack. In addition, all the carbon atoms are positively charged in A. They may be attacked by OH radical. Since we are interested in dehydrogenation reactions, all hydrogen atoms, and carbon atoms directly attached to hydrogens (C_2 and C_8), will be considered as OH radical attack sites.

Six different reaction pathways are found for [A + OH$^{\bullet}$ → reactant complexes → **TS** → product complexes → (A−H)$^{\bullet}$ + H_2O]. Ten intermediate adenine−OH complexes (**1**–**10**) and six transition states (**TS1**–**TS6**) for OH radical reacting with adenine are presented in Figures 5 and 6, respectively. The numbering schemes correspond to increasing energy, relative to separated adenine and OH radical. All energies are in kcal mol^{-1}, with ZPVE corrected values in parentheses. The energy profiles along the six pathways are displayed in Figure 7. For each pathway, optimized geometries of adenine-OH reactant complexes, transition states, and product complexes are shown in Figure 8–13. The corresponding relative energies are shown in these figures and in Table 2.

N_9 dehydrogenation: In the vicinity of the most positively charged hydrogen atom (H_9), the OH radical attaches to adenine through two hydrogen bonds (see Figure 8). This forms the reactant complex **9**, in which the hydrogen bond lengths of O···H_9 and N_3···H are 2.290 and 1.837 Å, respectively. As the reaction progresses from reactant complex **9**, the O···H_9 distance decreases to 1.367 Å in **TS2**, then to 0.980 Å in the product complex **2**. However, the N_9–H_9 bond length increases from 1.019 Å in the reactant complex **9**, to 1.147 Å at **TS2**, and finally to 1.957 Å in the product complex **2**.

For this reaction pathway (green in Figure 7), the reactant complex **9** has a binding energy of 10.66 (8.84 including

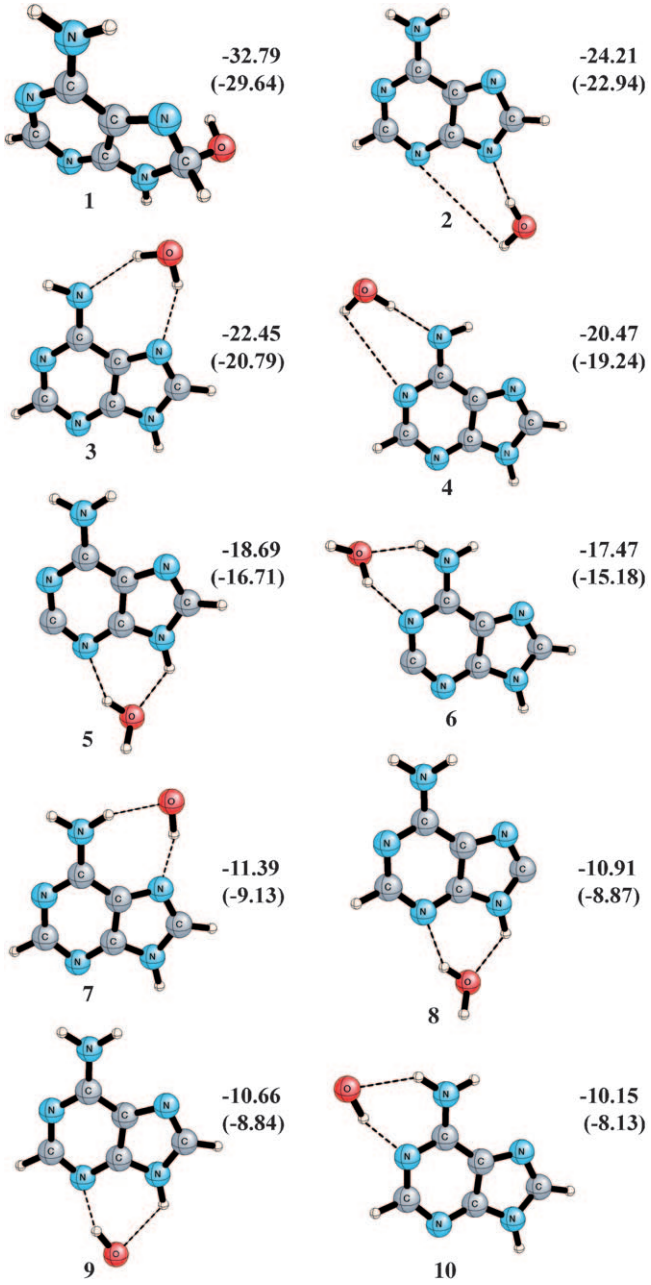

Figure 5. Numbering of the ten adenine−OH and (A−H)-H_2O radical complexes. Relative energies(in kcal mol^{-1}, ZPVE corrected values in parentheses) are indicated with respect to separated adenine and hydroxyl radical.

ZPVE) kcal mol^{-1} relative to separated adenine plus OH radical. The transition state **TS2** also lies below the separated reactants, by 3.68 (5.47) kcal mol^{-1}. The local barrier for this reaction pathway is predicted to be 6.98 (3.37) kcal mol^{-1} relative to reactant complex **9**. This is higher than the transition state for abstraction of H_{62}, but lower than that of H_{61} (discussed in the following sections). This reaction results in the lowest energy product complex **2**, which lies 24.21 (22.94) kcal mol^{-1} below separated adenine plus OH radical and 13.55 (14.10) kcal mol^{-1} lower in energy than re-

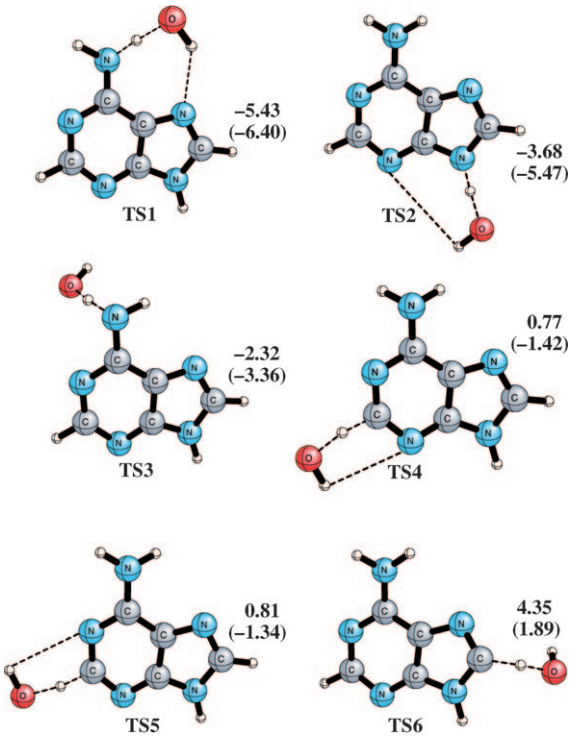

Figure 6. Numbering of the six A+OH→(A−H)+H_2O transition states. Relative energies (in kcal mol^{-1}, ZPVE corrected values in parentheses) are indicated with respect to separated adenine and hydroxyl radical.

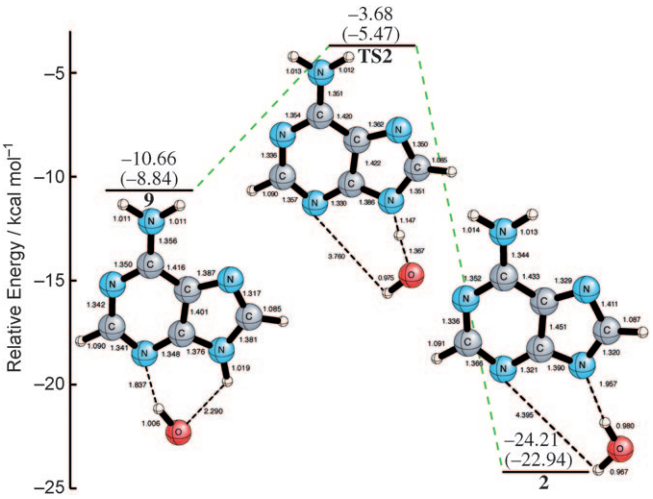

Figure 8. Optimized geometries for the hydroxyl radical attack on adenine position (N_9)H_9. Included in the figure are the reactant complex (**9**), transition state (**TS2**), and product complex (**2**). Bond lengths are in Å. Relative energies (in kcal mol^{-1}, ZPVE corrected values in parentheses) are given with respect to separated A+OH.

actant complex **9**. The dissociation energy for **2** is predicted to be 6.85 (5.06) kcal mol^{-1} with respect to separated (A−H_9)$^{\bullet}$ plus water. It should be noted that although H_9 is not present in nucleosides and nucleotides, N_9 dehydrogenation is still important for the experiments involving nucleobases.

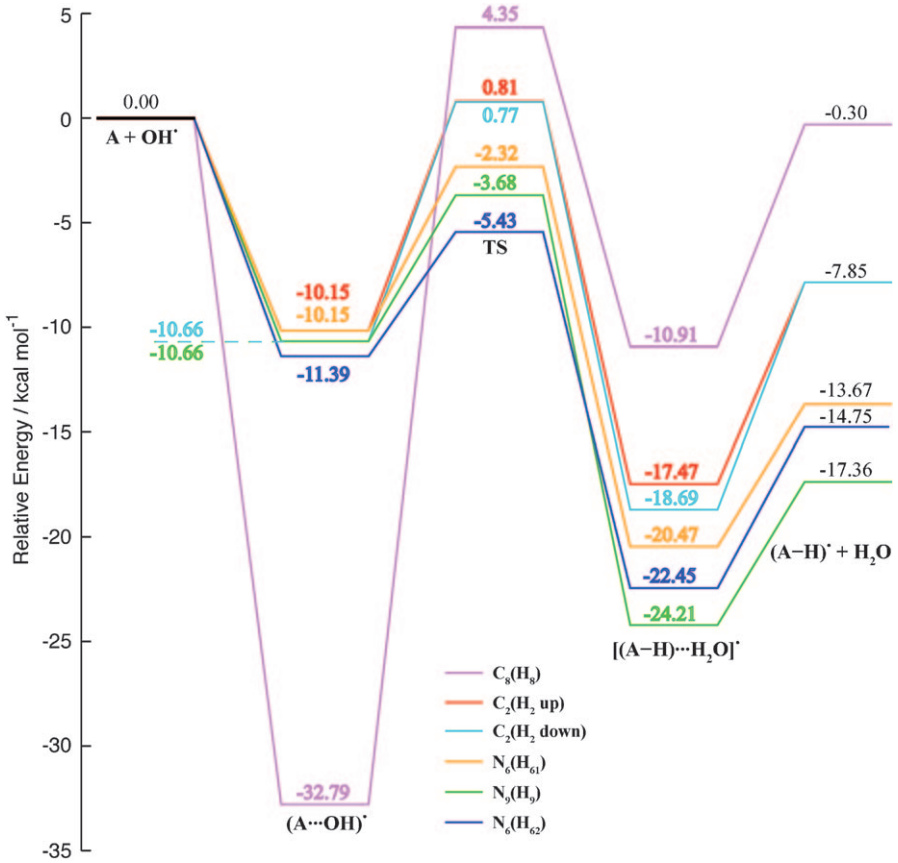

Figure 7. Relative energies (in kcal mol^{-1}) with respect to adenine and hydroxyl radical.

N_{62} dehydrogenation: Hydroxyl radical may also easily attack H_{62} (dark blue pathway, Figure 7), since it is the second most positively charged hydrogen atom in neutral adenine. The optimized geometries of the reactant complex **7**, transition state (**TS1**), and product complex **3** for this reaction pathway are presented in Figure 9. The N_6–H_{62} bond (1.021 Å) in **7** is only 0.01 Å longer than that in the isolated neutral adenine. H_{62} is hydrogen bonded to the attacking OH radical, with an O···H distance of 2.016 Å. The hydrogen of the hydroxyl radical links to N_7, forming another hydrogen bond with an H···N_7 distance of 1.792 Å. As the dehydrogenation reaction proceeds to **TS1**, the N_6–H_{62} bond lengthens to 1.155 Å, while the O···H_{62} distance decreases to 1.300 Å. When H_{62} is abstracted to form product complex **3**, the N_6···H_{62} distance further elongates to

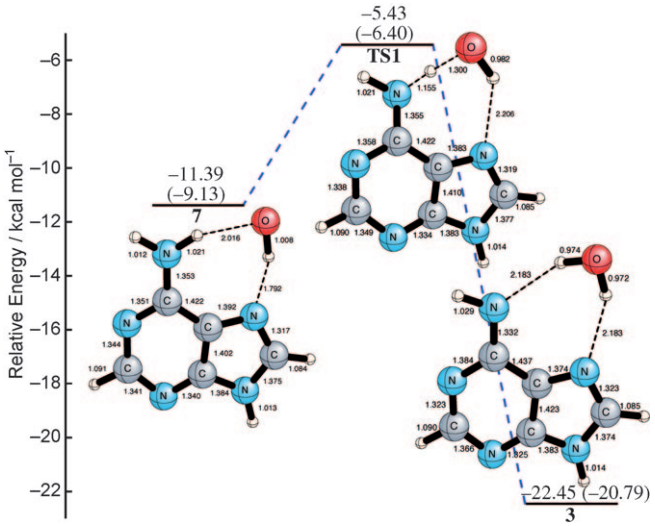

Figure 9. Optimized geometries for the hydroxyl radical attack on adenine position $(N_6)H_{62}$. Included in the figure are the reactant complex (**7**), transition state (**TS1**), and product complex (**3**). Bond lengths are in Å. Relative energies (in kcal mol^{-1}, ZPVE corrected values in parentheses) are given with respect to separated A + OH.

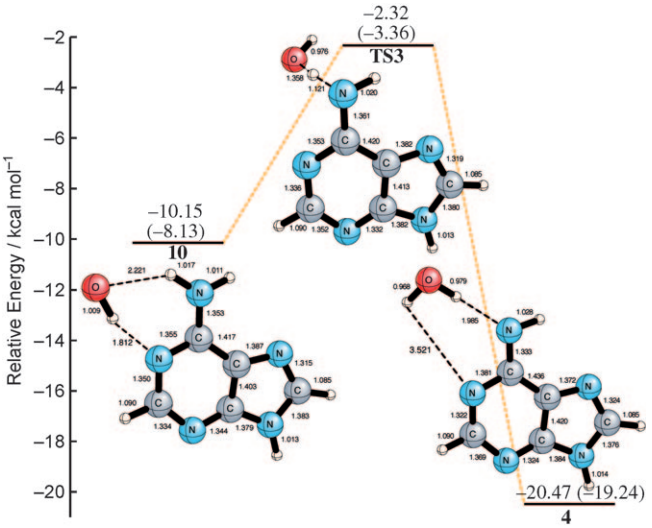

Figure 10. Optimized geometries for hydroxyl radical attack on adenine position $(N_6)H_{61}$. Included in the figure are the reactant complex (**10**), transition state (**TS3**), and product complex (**4**). Bond lengths are in Å. Relative energies (in kcal mol^{-1}, ZPVE corrected values in parentheses) are given with respect to separated A + OH.

2.183 Å, while the N_6–C_6 bond length shortens to 1.332 Å, i.e., by 0.02 Å compared to complex **7**. The O–H_{62} bond decreases to a normal water O–H bond (0.974 Å) in **3**.

The reactant complex **7** is stabilized by two hydrogen bonds. The binding energy between the adenine and the attacking OH radical is computed to be 11.39 (9.13 with ZPVE) kcal mol^{-1}. The local energy barrier (**7**→**TS1**) for the reaction is predicted to be 5.96 (2.72) kcal mol^{-1}. There is no barrier for this reaction pathway, since **TS1** lies 5.43 (6.40) kcal mol^{-1} below separated adenine plus OH radical. After H_{62} is abstracted, the resulting water and the newly formed (A–H)$^{\bullet}$ radical are held together by two hydrogen bonds, forming the [(A–H)···H_2O]$^{\bullet}$ product complex **3** with a binding energy of 22.45 (20.79) kcal mol^{-1} relative to the separated reactants. When **3** dissociates to separated products [$(A–H_{62})^{\bullet}$ + H_2O], the energy increases by 7.70 (5.52) kcal mol^{-1}. Compared to the reactant complex **7**, the product complex **3** is predicted to be 11.06 kcal mol^{-1} lower in energy. Thus, this dehydrogenation reaction energetically favors the [(A–H)···H_2O]$^{\bullet}$ complex.

N_{61} dehydrogenation: In order to attack H_{61} (orange pathway, Figure 7), the OH radical binds to adenine at the N_1 and N_6 positions through two hydrogen bonds, to form the reactant complex **10**. This reaction pathway proceeds through transition state **TS3** to form product complex **4** (Figure 10). The O···H_{61} distance in **10** is found to be 2.221 Å, a long hydrogen bond. The hydrogen in the hydroxyl radical is connected to N_1 with a hydrogen bond length of 1.812 Å. In **TS3**, the O···H_{61} separation decreases to 1.358 Å, and further shortens to 0.979 Å in the product complex **4**. Meanwhile, the N_6–H_{61} bond steadily increases along the reaction pathway, from 1.017 Å in **10**, to 1.121 Å in **TS3**, to 1.985 Å in **4**.

Let us now consider the energetics of the reaction A + OH → **10** → **TS3** → **4** → $(A–H_{61})^{\bullet}$ + H_2O. The binding energy for the reactant complex **10** is 10.15 (8.13) kcal mol^{-1} compared to the separated A plus OH reactants. The most important feature is that the energy of **TS3** lies 2.32 (3.36) kcal mol^{-1} below reactants A + OH$^{\bullet}$. The lack of any barrier with respect to reactants shows that this process should be facile. There is, of course, a barrier for the local approach of reactant complex **10** to **TS3**, and that barrier is 7.83 (4.77) kcal mol^{-1}. Meanwhile, the product complex **4** lies 10.33 (11.11) kcal mol^{-1} below **10**. Unlike the just-discussed N_{62} dehydrogenation product complex **3**, water and the (A–H)$^{\bullet}$ radical in **4** are held together only through one hydrogen bond. The corresponding dissociation energy is 6.80 kcal mol^{-1} relative to separated $(A–H_{61})^{\bullet}$ radical plus H_2O. The N_{61} dehydrogenation is comparable to N_{62} dehydrogenation thermodynamically. However, the two pathways are distinct, since the barrier to NH_2 rotation in adenine is about 14 kcal mol^{-1}. Interestingly, the barrier differs slightly based on the direction of rotation: 13.98 (13.58) or 14.53 (14.15) kcal mol^{-1}. However, experimental discrimination between these two pathways would require deuteration of H_{61} or H_{62}.

C_8 Dehydrogenation: The C_8 dehydrogenation pathway (magenta, Figure 7) involves reactant complex **1**, transition state **TS6**, and product complex **8** (see Figure 11). Although reactant complex **1** is a long-lived adduct, and has been characterized by experiment,[17,42,43] it will be termed a reactant complex for the sake of consistency. Oxygen bonds to C_8 directly in reactant complex **1**, instead of hydrogen bonding. This breaks the N_7=C_8 double bond and forms the low energy reactant complex **1**. Significant geometric changes

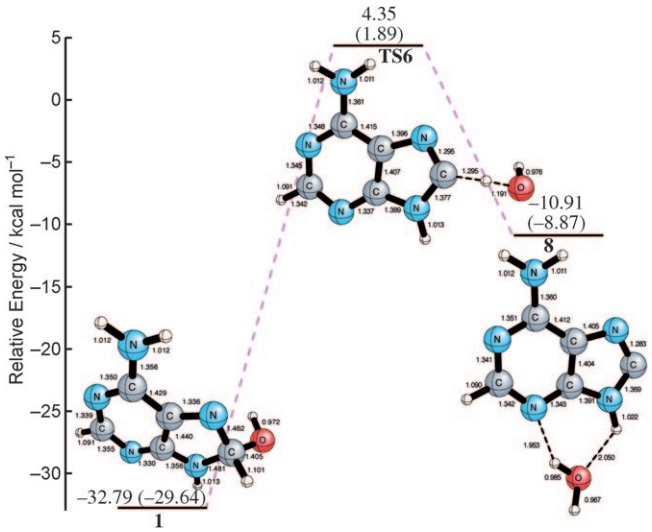

Figure 11. Optimized geometries for the hydroxyl radical attack on adenine position $(C_8)H_8$. Included in the figure are the reactant complex (**1**), transition state (**TS6**), and product complex (**8**). Bond lengths are in Å. Relative energies (in kcal mol^{-1}, ZPVE corrected values in parentheses) are given with respect to separated A + OH.

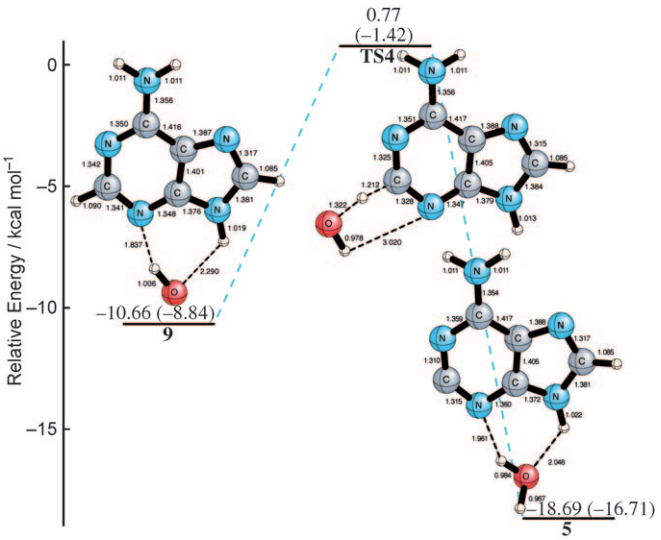

Figure 12. Optimized geometries for the hydroxyl radical attack on adenine position $(C_2)H_2$. Included in the figure are the reactant complex (**9**), transition state (**TS4**), and product complex (**5**). Bond lengths are in Å. Relative energies (in kcal mol^{-1}, ZPVE corrected values in parentheses) are given with respect to separated A + OH.

occur in the five and six-membered rings since the conjugation of the entire system has been disrupted. As the dehydration reaction proceeds, H_8 migrates away from C_8, forming a nearly linear (163.8°) C···H···O structure in **TS6**. In the product complex **8**, there are two hydrogen bonds; one of the hydrogen atoms from the newly formed water molecule hydrogen bonds to N_3 ($N\cdots H_8$ distance is 1.953 Å), while the oxygen hydrogen bonds to H_9 ($O\cdots H_9$ atomic distance is 2.050 Å).

Reactant complex **1** is extraordinarily stable; the binding energy (32.79 (29.64) kcal mol^{-1} relative to separated A + OH$^{\bullet}$) is much greater than that of the other dehydrogenation reactant complexes. However, dehydrogenation at C_8 is disfavored for several reasons. It is predicted to have a large local barrier (37.14 (31.53) kcal mol^{-1}) with respect to the reactant complex **1**. In addition, only this reaction pathway leads to a product complex (**8**) which lies above the corresponding reactant complex (**1**), by 21.88 (20.77) kcal mol^{-1}. Moreover, only the transition state (**TS6**) of this pathway lies appreciably (4.35 kcal mol^{-1}) above separated reactants A + OH$^{\bullet}$, indicating that C_8 dehydrogenation is unlikely at low temperatures. These energetics may explain the experimental inference that ring-opening, not dehydrogenation, occurs when OH radical attacks the C_8 position of adenine.[41,44]

C_2 dehydrogenation: Astraction of atom H_2 from adenine is complicated by the fact that two transition states **TS4** (Figure 12) and **TS5** (Figure 13) have been located (light blue and red pathways, in Figure 7). This indicates that there are two reaction pathways for C_2 dehydrogenation. **TS4** and **TS5** have similar geometries, except for the orientation of the OH radical. The energy difference between **TS4** and **TS5**, due to OH rotation, is only 0.04 (0.08) kcal mol^{-1}. In **TS4** and **TS5**, atom C_2, as discussed above (abstraction of H_8), is directly bonded to a hydrogen atom, so a reactant complex analogous to complex **1**, with OH radical directly attacking carbon, was considered. However, intrinsic reaction coordinate (IRC) analyses reveal that **TS4** connects the reactant complex **9** and the product complex **5**. Similarly, **TS5** connects the reactant complex **10** and the product complex **6**. This indicates that OH radical directly attacking C_2

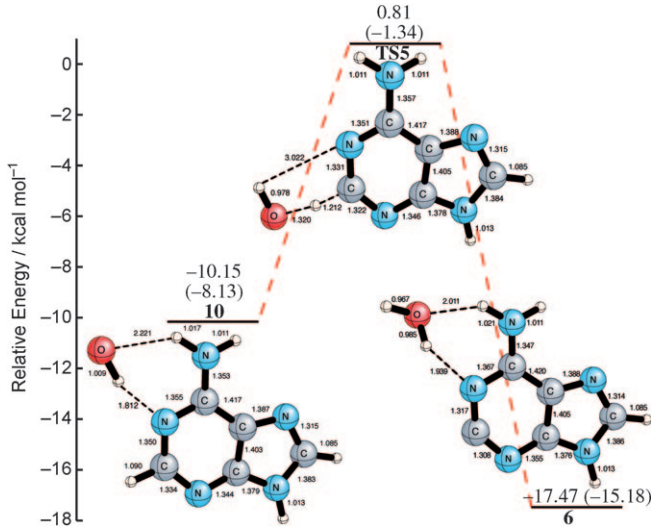

Figure 13. Optimized geometries for the hydroxyl radical attack on adenine position $(C_2)H_2$. Included in the figure are the reactant complex (**10**), transition state (**TS5**), and product complex (**6**). Bond lengths are in Å. Relative energies (in kcal mol^{-1}, ZPVE corrected values in parentheses) are given with respect to separated A + OH.

does not lead to dehydrogenation. In both product complexes **5** and **6**, two new hydrogen bonds are formed.

For these two reaction pathways, the reactant complexes are the same as in the N_9 and N_{61} dehydrogenations. The transition state **TS4** for hydroxyl H pointing "down" (Figure 12) lies 0.77 kcal mol^{-1} above separated A plus OH radical. The transition state **TS5** for hydroxyl H pointing "up" (Figure 13) lies 0.81 kcal mol^{-1} above the separated reactants. Inclusion of the ZPVE corrections decreases the energies to −1.34 and −1.42 kcal mol^{-1}. The local barriers for these two reaction pathways are predicted to be 11.42 (7.42) and 10.95 (6.79) kcal mol^{-1} relative to the reactant complexes **9** and **10**. Though these local barriers are not as high as for the C_8 dehydrogenation reaction, they are much higher than those for the N_9 and N_{61} dehydrogenations. The binding energies are 18.69 (16.71) and 17.47 (15.18) kcal mol^{-1} below separated adenine plus OH radical for product complexes **5** and **6**. The dissociation energies are predicted to be 10.84 (8.65) and 9.62 (7.12) kcal mol^{-1} for the two product complexes relative to separated $(A-H_2)^{\bullet}$ radical plus water.

Energetics: Table 3 reports the relative enthalpies, relative entropies and relative Gibbs energies for the six dehydrogenation reaction transition states. All energies are relative to separated adenine plus OH$^{\bullet}$ radical. The relative enthalpies and entropies are all negative for all the transition states. Therefore, low temperatures favor all these dehydrogenation reactions. There are two transition states with different OH orientation at the C_2 position, **TS4** and **TS5**. The reaction enthalpy barriers differ only by 0.02 kcal mol^{-1}, so these two reactions may happen simultaneously, based on the direction of the OH radical attack.

Table 2. Relative energies[a] (E_{rel}, in kcal mol^{-1}, ZPVE corrected values in parentheses) of sixteen structures with respect to separated adenine plus OH radical, and the dissociation energies (DE in kcal mol^{-1}, ZPVE corrected values in parentheses) with respect to separated dehydrogenated adenine radical plus water.

	Description	E_{rel} (A+OH)	DE (A−H)+H_2O
1	$[A_{H_8}\cdots OH]^{\bullet}$	−32.79 (−29.64)	32.49 (29.21)
2	$[(A-H)_{N_9}\cdots H_2O]^{\bullet}$	−24.21 (−22.94)	6.85 (5.06)
3	$[(A-H)_{N_{62}}\cdots H_2O]^{\bullet}$	−22.45 (−20.79)	7.70 (5.52)
4	$[(A-H)_{N_{61}}\cdots H_2O]^{\bullet}$	−20.47 (−19.24)	6.80 (5.04)
5[a]	$[(A-H)_{C_{21}}\cdots H_2O]^{\bullet}$	−18.69 (−16.71)	10.84 (8.65)
6[b]	$[(A-H)_{C_{22}}\cdots H_2O]^{\bullet}$	−17.47 (−15.81)	9.62 (7.12)
7	$[A_{H_{62}}\cdots OH]^{\bullet}$	−11.39 (−9.13)	−3.36 (−6.14)
8	$[(A-H)_{C_8}\cdots H_2O]^{\bullet}$	−10.91 (−8.87)	10.61 (8.44)
9	$[A_{H_9}\cdots OH]^{\bullet}$	−10.66 (−8.84)	−6.71 (−9.04)
10	$[A_{H_{61}}\cdots OH]^{\bullet}$	−10.15 (−8.13)	−3.52 (−6.07)
TS1	N_{62} position	−5.43 (−6.40)	−9.31 (−8.87)
TS2	N_9 position	−3.68 (−5.47)	−13.68 (−12.41)
TS3	N_{61} position	−2.32 (−3.36)	−11.35 (−10.85)
TS4[b]	C_{21} position	0.77 (−1.42)	−8.61 (−6.64)
TS5[c]	C_{22} position	0.81 (−1.34)	−8.65 (−6.72)
TS6	C_8 position	4.35 (1.89)	−4.65 (−2.31)

[a] These are also the negative values of binding energies. [b] C_{21} is for transition state and product of C_2 position reaction with a lower energy, see Figure 10. [c] C_{22} is for transition state and product of C_2 position reaction with a higher energy, see Figure 11.

Table 3. Barrier heights ($\Delta H^{\neq}$, in kcal mol^{-1}), barrier entropy changes ($\Delta S^{\neq}$, in cal mol^{-1}) and ordered Gibbs energies of activation ($\Delta G^{\neq}$, in kcal mol^{-1}) with respect to separated adenine plus OH radical at 298.18 K for the six dehydrogenation reactions [A+OH$^{\bullet}$→TS→(A−H)$^{\bullet}$+H_2O].

	$\Delta H^{\neq}$	$\Delta S^{\neq}$	$\Delta G^{\neq}$
TS1 (N_{62} position)	−2.06	−32.67	7.68
TS2 (N_9 position)	−2.32	−28.00	6.03
TS3 (N_{61} position)	−1.81	−29.47	6.98
TS4 (C_{21} position)	−2.51	−26.22	5.31
TS5 (C_{22} position)	−2.53	−27.03	5.53
TS6 (C_8 position)	−2.79	−27.13	5.29

The energy profiles along the six reaction pathways (A+OH→reactant complexes→**TS**→product complexes→(A−H)$^{\bullet}$+H_2O) are shown in Figure 7. The most important feature is that all the transition states lie near or below separated A+OH$^{\bullet}$ in energy, except for **TS6** on the C_8 pathway. The lack of any barrier with respect to reactants shows that these processes, except for C_8 dehydrogenation, should be facile. Based on the transition state energies, the dehydrogenation of $N_{62}(H_{62})$ is the most kinetically favorable reaction pathway with a transition state lying 5.43 kcal mol^{-1} below separated adenine plus OH radical. It is followed by N_9 and $N_6(H_{61})$ dehydrogenation (3.68 and 2.32 kcal mol^{-1}, respectively, below separated reactants). The C_2 dehydrogenation transition state energies vary based on hydroxyl orientation; 0.77 and 0.81 kcal mol^{-1} above separated reactants, for H from hydroxyl radical pointing "down" and "up", respectively. Note that with the ZPVE correction these transition states lie below the separated reactants. Dehydrogenation at the C_8 site is energetically least favored, with a transition state 4.35 kcal mol^{-1} above separated adenine plus OH radical.

Optical transitions: TD-DFT computed absorption spectra for adenine, the four reactant complexes, and the five dehydrogenated adenine radicals are shown in Table 4. In this context Vieira and Steenken[41] recorded optical absorption spectra in the 250–700 nm region. Their initial spectrum was measured 2 μs after the reaction of OH radical with adenine. Additional spectra were recorded 30 μs after completion of the first-order transformation reaction.

The laboratory spectrum recorded 2 μs after the reaction showed small peaks around 300 and 400 nm, with a broad peak from 450–600 nm. In our computations, the N_9-, N_{61}-, and N_{62}-dehydrogenated adenine radicals have strong transitions in the 300 nm region. For N_9, the main transitions are at 302 nm (f=0.050), 312 nm (f=0.068); for N_{61}, 298 nm (f=0.080); and for N_{62}, 300 nm (f=0.079). These products were not mentioned in Vieira and Steenken's work. Vieira and Steenken assigned the features around 400 nm to the dehydration reaction of the A4OH radical.[41] However, the $^{\bullet}$OH+A→A4OH$^{\bullet}$→A−$H_6^{\bullet}$+H_2O reaction was not considered in our work, since the mechanism involves a complex series of proton transfers. Our TD-DFT computations indicate that N_{61}- and N_{62}-dehydrogenated adenine radical prod-

Table 4. Vertical optical transitions (absorption spectra λ in nm) of the adenine molecule, four reactant complexes, and five dehydrogenated adenine radicals, predicted using the TD-DFT approach. Oscillator strengths (f) are reported for transitions ≥ 0.010 in magnitude.

	λ (f)	λ (f)	λ (f)	λ (f)	λ (f)	λ (f)	λ (f)	λ (f)
adenine	203 (0.096)	204 (0.035)	239 (0.034)	250 (0.202)				
1 C_8 site reactant complex	242 (0.068)	244 (0.035)	245 (0.018)	260 (0.022)	313 (0.135)	335 (0.032)	451 (0.013)	
9 N_9 site reactant complex	238 (0.038)	250 (0.221)						
10 N_{61} site reactant complex	241 (0.070)	251 (0.206)						
7 N_{62} site reactant complex	240 (0.036)	258 (0.187)						
C_2-dehydrogenated A	245 (0.207)	259 (0.010)						
C_8-dehydrogenated A	228 (0.019)	237 (0.112)	241 (0.080)	247 (0.014)				
N_9-dehydrogenated A	242 (0.037)	259 (0.024)	277 (0.019)	302 (0.050)	312 (0.068)	522 (0.033)		
N_{61}-dehydrogenated A	250 (0.024)	277 (0.016)	298 (0.080)	421 (0.017)	505 (0.034)			
N_{62}-dehydrogenated A	222 (0.025)	229 (0.048)	252 (0.052)	261 (0.031)	279 (0.022)	300 (0.079)	427 (0.015)	506 (0.036)

ucts have optical transitions in this region; that is, $\lambda =$ 421 nm ($f=0.017$) and $\lambda = 427$ nm ($f=0.015$), respectively.

After 30 μs, the Vieira-Steenken spectrum showed a significant increase of optical density (OD) at about 330 nm, compared to the 2 μs spectrum. This feature was assigned by Steenken to the ring-opening reaction of A8OH radical. There is also a very broad, though weak, peak in the 450–700 nm region. As mentioned above, the N_{61}- and N_{62}-dehydrogenated adenine radicals have transitions in this region. However, none of these transitions is very strong. The C_8 reactant complex **1** does have a strong transition at 313 nm ($f=0.135$); see Table 4. It has a significant shoulder at a higher wavelength (335 nm, $f=0.032$) and several weak shoulders in the 242–451 nm region. This peak cannot be definitively assigned, since we focused on dehydrogenation reactions of adenine in this work. The ring-opening reaction transients and products, as mentioned before,[40,41,44–46] may present strong transitions corresponding to these shorter wavelength peaks.

Conclusion

Six possible dehydrogenation reaction pathways for adenine attacked by the hydroxyl radical have been investigated at the B3LYP/DZP++ level of theory. The N_{62}, N_9, and N_{61} pathways have transition states lower in energy than separated adenine and hydroxyl radical; −5.43, −3.68, and −2.32 kcal mol^{-1}, respectively. After including the ZPVE corrections, only the C_8 dehydrogenation transition state is higher in energy than the separated reactants. This suggests that, except for attacking at the C_8 site, OH radical attack at all other positions will lead to dehydrogenation spontaneously, forming an adenine radical and water. Based on energetic analyses, the reactions at N_9, N_{61}, and N_{62} are exothermic, while those at C_2 and C_8 are endothermic. Since N_{62} has the lowest lying transition state, it is the most kinetically favorable pathway for dehydrogenation. Other compatible pathways are the dehydrogenation at N_9 and N_{61}. Dehydrogenation at C_2 is less favorable than at the N_9 and N_{61} positions. For the C_8 pathway, though the activation energy is 4.35 kcal mol^{-1} relative to separated A plus OH radical, the local barrier is 37.14 kcal mol^{-1} with respect to reactant complex **1**. These relatively high barriers indicate that C_8 dehydrogenation is unlikely to take place; ring-opening reaction may occur in agreement with early experiments.[41,44] The TD-DFT computed transitions of N_{61} at 421 nm and N_{62} 427 nm agree well with the early experimental assignment of a 400 nm band to dehydrogenation at N_6 position. The N_6 position is most favorable for OH radical attack, leading to formation of N_6-dehydrogenated adenine radicals.

Acknowledgements

The authors would like to thank Heather M. Jaeger, Dr. Francesco A. Evangelista and Dr. Yaoming Xie for insightful discussions and technical expertise. This research was funded by the U.S. National Science Foundation, Grant CHE-0749868.

[1] D. K. Hazra, S. Steenken, *J. Am. Chem. Soc.* **1983**, *105*, 4380.
[2] E. Sagstuen, E. O. Hole, W. H. Nelson, D. M. Close, *J. Phys. Chem.* **1992**, *96*, 1121.
[3] E. Sagstuen, E. O. Hole, W. H. Nelson, D. M. Close, *J. Phys. Chem.* **1992**, *96*, 8269.
[4] D. M. Close, *Radiat. Res.* **1993**, *135*, 1.
[5] A. O. Colson, M. D. Sevilla, *J. Phys. Chem.* **1995**, *99*, 13033.
[6] D. M. Close, L. A. Eriksson, E. O. Hole, E. Sagstuen, W. H. Nelson, *J. Phys. Chem. B* **2000**, *104*, 9343.
[7] M. Krauss, R. Osman, *J. Phys. Chem. A* **1997**, *101*, 4117.
[8] A. O. Colson, D. Becker, I. Eliezer, M. D. Sevilla, *J. Phys. Chem. A* **1997**, *101*, 8935.
[9] S. Steenken, S. V. Jovanovic, *J. Am. Chem. Soc.* **1997**, *119*, 617.
[10] S. D. Wetmore, R. J. Boyd, *J. Phys. Chem. B* **1998**, *102*, 9332.
[11] S. D. Wetmore, F. Himo, R. J. Boyd, L. A. Eriksson, *J. Phys. Chem. B* **1998**, *102*, 7484.
[12] S. D. Wetmore, R. J. Boyd, L. A. Eriksson, *J. Phys. Chem. B* **1998**, *102*, 10602.
[13] S. D. Wetmore, R. J. Boyd, L. A. Eriksson, *J. Phys. Chem. B* **1998**, *102*, 5369.
[14] S. D. Wetmore, R. J. Boyd, F. Himo, L. A. Eriksson, *J. Phys. Chem. B* **1999**, *103*, 3051.
[15] S. D. Wetmore, R. J. Boyd, L. A. Eriksson, *Chem. Phys. Lett.* **2000**, *322*, 129.
[16] J. Cadet, T. Delatour, T. Douki, D. Gasparutto, J. P. Pouget, J. L. Ravanat, S. Sauvaigo, *Mutat. Res.* **1999**, *424*, 9.
[17] L. P. Candeias, S. Steenken, *Chem. Eur. J.* **2000**, *6*, 475.
[18] S. S. Wallace, *Free Radical Biol. Med.* **2002**, *33*, 1.

[19] C. J. Mundy, M. E. Colvin, A. A. Quong, *J. Phys. Chem. A* **2002**, *106*, 10063.
[20] R. Kakkar, R. Garg, *J. Mol. Struct.* **2003**, *644–686*, 139.
[21] Y. Wu, C. J. Mundy, M. E. Colvin, R. Car, *J. Phys. Chem. A* **2004**, *108*, 2922.
[22] K. C. Hunter, L. R. Rutledge, S. D. Wetmore, *J. Phys. Chem. A* **2005**, *109*, 9554.
[23] M. H. Almatarneh, C. G. Flinn, R. Poirier, *J. Phys. Chem. A* **2006**, *110*, 8227.
[24] R. B. Zhang, L. A. Eriksson, *J. Phys. Chem. B* **2007**, *111*, 6571.
[25] J. D. Zhang, H. F. Schaefer, *J. Chem. Theory Comput.* **2007**, *3*, 115.
[26] M. H. Almatarneh, C. G. Flinn, R. Poirier, *J. Chem. Inf. Model* **2008**, *48*, 831.
[27] R. H. Duncan Lyngdoh, H. F. Schaefer, *Acc. Chem. Res.* **2009**, *42*, 563.
[28] A. Kumar, M. D. Sevilla, *Chem. Rev.* DOI:10.1021/cr100023g .
[29] B. Halliwell, I. Okezie, E. Aruoma, *DNA and Free Radicals*, 2nd ed., Ellis Horwood, New York, **1993**.
[30] C. Von Sonntag, *The Chemical Basis of Radiation Biology*, Taylor & Franci, London, **1987**.
[31] M. Dizdaroglu, *Free Radical Biol. Med.* **1991**, *10*, 225.
[32] N. L. Oleinick, S. Cluh, N. Ramakrishman, L. Xue, *Br. J. Cancer* **1987**, *55*, Suppl. VIII 135.
[33] B. Halliwell, J. M. C. Gutteridge, *Free Radicals in Biology and Medicine*, Clarendon Press, Oxford, **1989**.
[34] A. J. Bertinchamps, J. Hüttermann, W. Köhnlein, R. Teoule, *Effects of Ionizing Radiation on DNA*, Springer, Berlin, **1987**.
[35] W. A. Bernhard, *Adv. Radiat. Biol.* **1981**, *9*, 199.
[36] J. P. Pouget, S. Frelon, J. L. Ravanat, I. Testard, F. Odin, J. Cadet, *Radiat. Res.* **2002**, *157*, 589.
[37] J. Cadet, E. Sage, T. Douki, *Mutat. Res.* **2005**, *571*, 3.
[38] B. Aydogan, W. E. Bolch, S. G. Swarts, J. E. Turner, D. T. Marshall, *Radiat. Res.* **2008**, *169*, 223.
[39] C. Chatgilialoglu, M. D'Angelantonio, M. Guerra, P. Kaloudis, Q. G. Mulazzani, *Angew. Chem.* **2009**, *121*, 2248; *Angew. Chem. Int. Ed.* **2009**, *48*, 2214.
[40] S. Steenken, *Chem. Rev.* **1989**, *89*, 503.
[41] A. J. S. C. Vieira, S. Steenken, *J. Am. Chem. Soc.* **1990**, *112*, 6986.
[42] A. J. S. C. Vieira, S. Steenken, *J. Phys. Chem.* **1991**, *95*, 9340.
[43] P. O'Neill, *Radiat. Res.* **1983**, *96*, 198.
[44] A. J. S. C. Vieira, S. Steenken, *J. Phys. Chem.* **1987**, *91*, 4138.
[45] J. Llano, L. A. Eriksson, *Phys. Chem. Chem. Phys.* **2004**, *6*, 4707.
[46] S. Naumov, C. V. Sonntag, *Radiat. Res.* **2008**, *169*, 355.
[47] E. O. Hole, E. Sagstuen, W. H. Nelson, D. M. Close, *Radiat. Res.* **1995**, *144*, 258.
[48] D. M. Close, W. H. Nelson, *Radiat. Res.* **1989**, *117*, 367.
[49] W. H. Nelson, E. Sagstuen, E. O. Hole, D. M. Close, *Radiat. Res.* **1992**, *131*, 272.
[50] L. Kar, W. A. Bernhard, *Radiat. Res.* **1983**, *93*, 232.
[51] H. Xie, Z. Cao, *Int. J. Quantum Chem.* **2007**, *107*, 1261.
[52] M. E. Harding, J. Vásquez, B. Ruscic, A. K. Wilson, J. Gauss, J. F. Stanton, *J. Chem. Phys.* **2008**, *128*, 114111.
[53] A. Karton, E. Rabinovich, J. M. Martin, B. Ruscic, *J. Chem. Phys.* **2006**, *125*, 144108.
[54] Y. Shao, C. Saravanan, M. H. Gordon, C. White, *J. Chem. Phys.* **2003**, *118*, 6144.
[55] P. Salek, S. Høst, L. Thøgersen, P. Jørgensen, P. Manninen, J. Olsen, B. Jansík, S. Reine, F. PawŃoski, E. Tellgren, T. Helgaker, S. Coriani, *J. Chem. Phys.* **2007**, *126*, 114110.
[56] S. Wang, H. F. Schaefer, *J. Chem. Phys.* **2006**, *124*, 044303.
[57] F. A. Evangelista, A. Paul, H. F. Schaefer, *J. Phys. Chem. A* **2004**, *108*, 3565.
[58] S. S. Wesolowski, M. L. Leininger, P. N. Pentchev, H. F. Schaefer, *J. Am. Chem. Soc.* **2001**, *123*, 4023.
[59] N. A. Richardson, S. S. Wesolowski, H. F. Schaefer, *J. Am. Chem. Soc.* **2002**, *124*, 10163.
[60] N. A. Richardson, S. S. Wesolowski, H. F. Schaefer, *J. Phys. Chem. B* **2003**, *107*, 848.
[61] N. A. Richardson, J. Gu, S. Wang, Y. Xie, H. F. Schaefer, *J. Am. Chem. Soc.* **2004**, *126*, 4404.
[62] A. D. Becke, *J. Chem. Phys.* **1993**, *98*, 5648.
[63] C. Lee, W. Yang, R. G. Parr, *Phys. Rev. B* **1988**, *37*, 785.
[64] T. J. Lee, H. F. Schaefer, *J. Chem. Phys.* **1985**, *83*, 1784.
[65] J. C. Rienstra-Kiracofe, G. S. Tschumper, H. F. Schaefer, S. Nandi, G. B. Ellison, *Chem. Rev.* **2002**, *102*, 231.
[66] A. E. Reed, F. Weinhold, *J. Chem. Phys.* **1983**, *78*, 4066.
[67] A. E. Reed, R. B. Weinstock, F. Weinhold, *J. Chem. Phys.* **1985**, *83*, 735.
[68] A. Szabo, N. S. Ostlund, *Modern Quantum Chemistry: Introduction To Advanced Electronic Structure Theory*, Dover, New York, **1998**.
[69] H. F. Schaefer, *Chem. Br.* **1975**, *11*, 227.
[70] K. Fukui, *Acc. Chem. Res.* **1981**, *14*, 363.
[71] M. W. Schmidt, M. S. Gordon, M. Dupuis, *J. Am. Chem. Soc.* **1985**, *107*, 2585.
[72] B. C. Garrett, J. Redmon, M. R. Steckler, D. G. Truhlar, K. K. Baldridge, D. Bartol, M. W. Schmidt, M. S. Gordon, *J. Phys. Chem.* **1988**, *92*, 1476.
[73] Y. Shao, L. Fusti-Molnar, Y. Jung, J. Kussmann, C. Ochsenfeld, S. T. Brown, A. T. B. Gilbert, L. V. Slipchenko, S. V. Levchenko, D. P. O'Neill, R. A. D. , Jr., R. C. Lochan, T. Wang, G. J. O. Beran, N. A. Besley, J. M. Herbert, C. Y. Lin, T. V. Voorhis, S. H. Chien, A. Sodt, R. P. Steele, V. A. Rassolov, P. E. Maslen, P. P. Korambath, R. D. Adamson, B. Austin, J. Baker, E. F. C. Byrd, H. Dachsel, R. J. Doerksen, A. Dreuw, B. D. Dunietz, A. D. Dutoi, T. R. Furlani, S. R. Gwaltney, A. Heyden, S. Hirata, C. P. Hsu, G. Kedziora, R. Z. Khalliulin, P. Klunzinger, A. M. Lee, M. S. Lee, W. Liang, I. Lotan, N. Nair, B. Peters, E. I. Proynov, P. A. Pieniazek, Y. M. Rhee, J. Ritchie, E. Rosta, C. D. Sherrill, A. C. Simmonett, J. E. Subotnik, H. L. W. III, W. Zhang, A. T. Bell, A. K. Chakraborty, D. M. Chipman, F. J. Keil, A. Warshel, W. J. Hehre, H. F. Schaefer, J. Kong, A. I. Krylov, P. M. W. Gill, M. Head-Gordon, *Phys. Chem. Chem. Phys.* **2006**, *8*, 3172.

Received: May 7, 2010
Published online: September 28, 2010

